Quantitative STEM Imaging of Order-Disorder Phenomena in Double Perovskite Thin Films

B. D. Esser,[1] A. J. Hauser,[2] R. E. A. Williams,[1] L. J. Allen,[3] P. M. Woodward,[4] F. Y. Yang,[2] and D. W. McComb[1]
[1]Department of Materials Science and Engineering, The Ohio State University, Columbus, Ohio 43210, USA
[2]Department of Physics, The Ohio State University, Columbus, Ohio 43210, USA
[3]School of Physics, University of Melbourne, Parkville, Victoria 3010, Australia
[4]Department of Chemistry, The Ohio State University, Columbus, Ohio 43210, USA
(Received 8 June 2016; revised manuscript received 29 August 2016; published 20 October 2016)

Using aberration-corrected high-angle annular dark field scanning transmission electron microscopy (HAADF-STEM), we investigate ordering phenomena in epitaxial thin films of the double perovskite Sr_2CrReO_6. Experimental and simulated imaging and diffraction are used to identify antiphase domains in the films. Image simulation provides insight into the effects of atomic-scale ordering along the beam direction on HAADF-STEM intensity. We show that probe channeling results in ±20% variation in intensity for a given composition, allowing 3D ordering information to be probed using quantitative STEM.

DOI: 10.1103/PhysRevLett.117.176101

Half-metallic double perovskites of the general formula $A_2BB'O_6$ are of great interest for their possible application in spintronic devices, because they exhibit ferrimagnetism with high Curie temperatures (T_C) and a high degree of spin polarization [1,2]. One current obstacle to their use is the ability to grow the materials in the form of high-quality films with minimal antisite disorder [3]. Many factors can influence and modify the properties of double perovskites in thin film form, including lattice strain [4], degree of chemical ordering [5], the presence of defects [6], etc. Further investigation into these phenomena is necessary to fully realize thin film double perovskites and the next generation of electronic devices.

The B and B' cations can be distributed in an ordered array or randomly on the B-site sublattice of the perovskite structure. The degree of B/B' ordering is important due to the effect that it can have on the electronic and magnetic properties of double perovskites [3,7–13]. In general, double perovskites must exhibit a high degree of B/B' ordering in order to achieve their high T_C and high spin polarization [3]. Thus, it is important to quantify the degree of B/B' ordering in thin films at the atomic scale. This can be achieved through the use of quantitative aberration-corrected scanning transmission electron microscopy (STEM).

By carefully controlling experimental factors such as sample preparation and microscope conditions, quantitative comparisons have been made possible between experiment and simulation. Quantitative STEM has been used to achieve atom counting in the beam direction [14], location of individual dopant atoms in three dimensions [15,16], and characterization of chemical ordering on the atomic scale [17–20]. All of these methods have relied on the intensity of atomic columns in high-angle annular dark field (HAADF) STEM images. In this Letter, we will show that additional parameters, including specimen thickness and atomic-scale compositional analysis, are necessary in combination with simulations to characterize atomic-scale ordering along the path of the electron beam.

It was previously reported through Rietveld refinement of x-ray diffraction (XRD) data that thin films of the double perovskite Sr_2CrReO_6 (SCRO) grown on (001)-oriented $SrTiO_3$ (STO) with a 50 nm buffer layer of relaxed $SrCr_{0.5}Nb_{0.5}O_3$ showed an exceptionally high ordering parameter $\eta = 0.99 \pm 0.01$ [21]. An ordering parameter this close to unity indicates that nearly all of the Cr and Re atoms are perfectly ordered on the B/B' sites—leading to a superlattice of (111) planes of B and B' ions that is equivalent to a rocksalt structure. At room temperature, the stable SCRO structure is tetragonal ($I4/m$, $a = 5.569$ Å, $c = 7.804$ Å) [4] and has a well-defined orientation relation to the STO substrate, namely, $SCRO_{\langle 100\rangle}||STO_{\langle 110\rangle}$ and $SCRO_{\langle 001\rangle}\,||\,STO_{\langle 001\rangle}$ [21].

As reported in our previous studies, epitaxial SCRO(001) films were grown on STO(001) by ultrahigh vacuum off-axis sputtering [4,21]. In the current study, we prepared cross-sectional TEM samples of the 190 nm thick SCRO film from Ref. [21] using an FEI Helios NanoLab 600 DualBeam focused ion beam (FIB) with 30 kV and then 5 kV Ga ions. Final cleaning passes were performed in a Fischione Nanomill with 900 V and then 500 V Ar ions to remove any amorphous damage layers created in the FIB. The thickness of the specimen in the electron beam direction was measured to be approximately 8 nm by position-averaged convergent beam electron diffraction [22]. Imaging was performed on an FEI Titan^3 80-300 probe-corrected STEM at 300 kV. The use of a probe corrector limits the size of the electron probe to less than 100 pm, resulting in high-quality, high spatial resolution STEM images. When imaged in the HAADF-STEM condition with a collection range of approximately 55–375 mrad, the fully

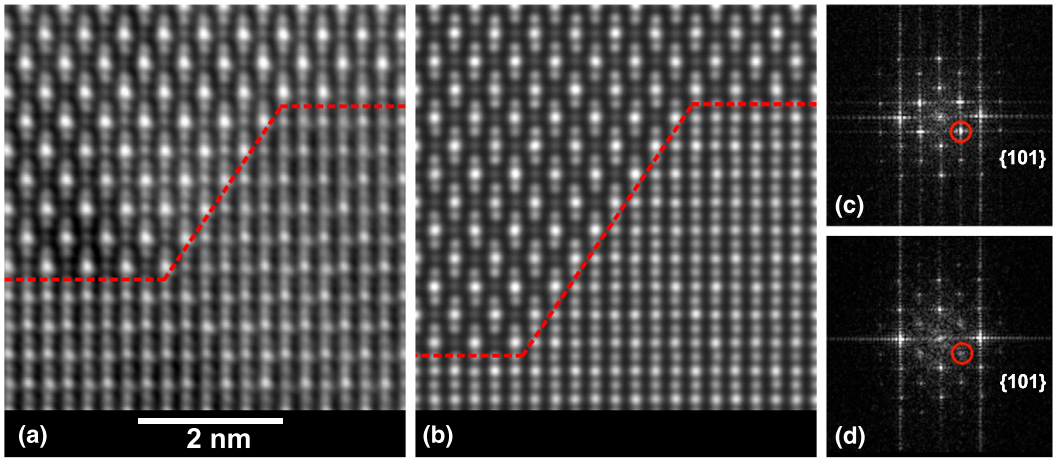

FIG. 1. Experimental (a) and simulated (b) HAADF-STEM images of an ordered region of SCRO (top) with antiphase domains (APDs) (bottom) separated by the red dashed line. FFT of the ordered (c) and APD (d) regions showing the decrease of intensity on the {101}-type superlattice reflections.

ordered double perovskite structure of SCRO should exhibit clear intensity variations when viewed along the [100] direction due to the individual columns of Cr, Sr/O, and Re. HAADF-STEM imaging provides Z contrast, where Z is the atomic number, such that the Cr columns exhibit the lowest intensity while the Re columns show the highest. It was noteworthy that some regions in the SCRO films, mostly near the interface, exhibited contrast that did not appear to be well ordered in spite of the previously published XRD data of Hauser *et al.*, which indicated that these same films were highly ordered over the entire sample [21]. Additionally, overall contrast was lower in these regions, as seen in the lower right-hand portion of Fig. 1(a). This STEM observation would suggest that there is a much lower degree of Cr/Re ordering within the films than previously reported, which would have significant (negative) implications for their properties.

After careful examination of many different regions within the SCRO thin films, it was concluded that the decrease in overall contrast within these seemingly disordered regions was unlikely to be a consequence of chemical disorder given the facetted or linear nature of the boundaries between what appeared to be ordered and disordered regions, as shown in Fig. 1(a). The most likely reason for the observed structure was that the overall reduction in contrast was due to antiphase domains in the SCRO thin films, leading to a misregistry of the Cr and Re columns, as shown in Fig. 2, leaving both Sr and O on equivalent sites. This misregistry is the proposed reason for the reduction in contrast in some regions of the thin films, because it would result in columns of Sr/O and mixed Cr/Re. The average atomic weight of the mixed Cr/Re columns would then be a weighted average based on the location of the antiphase boundary within the thickness of the TEM foil.

In order to understand the observed contrast variation in both the ordered and antiphase domains, HAADF-STEM image simulations were performed using the quantum excitation of phonons model [23,24]. A crystal model was prepared using a supercell of SCRO in which a $\frac{1}{2}[001]$ on (100) antiphase domain was created midway through the thickness normal to the viewing direction to simulate the lower-contrast region, as shown in Fig. 2(a). To match the observed experimental images, there must also be a second antiphase boundary parallel to the viewing direction that forms a boundary between the high- and low-contrast regions, as seen in Fig. 2(b). Thus, the supercell contained a region where clear B/B' ordering led to distinct contrast variation and a region where the intensity from the B/B' columns due to antiphase domains was less distinct. Since the supercell was not periodic in nature, it was simulated with 5 Å of vacuum around it in the plane normal to the viewing direction. The supercell was made to be approximately 55 Å thick to simulate a thin STEM specimen and sliced such that each projected potential contained a single plane of atoms—approximately 1.4 Å in thickness. Imaging conditions similar to those used in the probe-corrected Titan[3] were used, specifically 300 kV accelerating voltage, a beam convergence semiangle of 20 mrad, and aberration coefficients obtained from the microscope corrector software [C_3 and C_5 of 2 μm and 1 mm, respectively]. Further information about microscope details can be found in Ref. [25]. A finite source size with a 0.8 Å full width at half maximum Gaussian as well as detector shot noise of approximately 2% were incorporated in a simulated image at zero defocus [26], showing very good qualitative agreement with the contrast observed in experimental images of the films, as seen in Fig. 1(b).

To further confirm the hypothesis that the observed contrast is due to antiphase domains and not random B/B' disorder, electron diffraction patterns were simulated using multislice simulations for the fully ordered SCRO structure and for a supercell containing an antiphase domain.

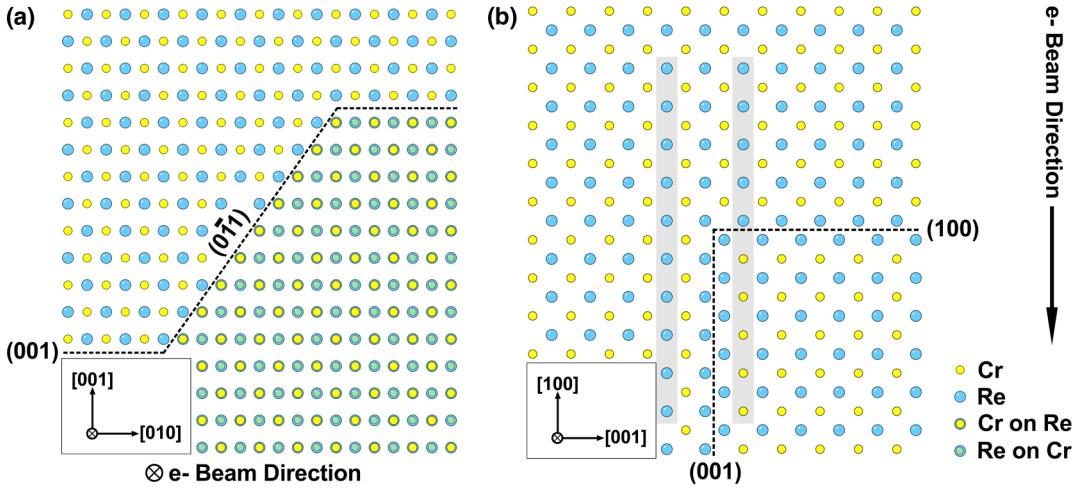

FIG. 2. Schematic showing the geometry of the antiphase domain image. Antiphase boundaries indicated by dashed lines. (a) Plan view, [100], schematic (corresponds to HAADF image in Fig. 1); (b) side view, [010], showing pure Re, or Cr, columns (highlighted) outside of the antiphase domain, and mixed occupancy columns that switch from Re to Cr atoms, or vice versa, across the antiphase boundary (highlighted). Sr and O atoms are omitted for clarity.

The results showed that, in perfectly ordered SCRO ($\eta = 1$), $\{101\}$-type superlattice reflections should be clearly visible in the diffraction pattern. Conversely, in the supercell containing an antiphase domain, the intensity of the superlattice reflections is significantly reduced. For reference, the SCRO structure where Cr and Re are fully disordered (randomly distributed among the B and B' sites) results in a diffraction pattern with no $\{101\}$-type superlattice reflections due to structure factor considerations.

The simulation of diffraction patterns for SCRO with different ordering parameters illustrates that by using experimental diffraction patterns it is possible to differentiate between low-contrast regions in the HAADF-STEM image exhibiting high degrees of disorder and those that are a consequence of antiphase domains. Diffraction work was attempted on TEM samples prepared using a dual-beam FIB; however, small variations in tilt across the sample due to the thin foil geometry and FIB process resulted in subtle changes in contrast in the diffracted beams, making any definitive analysis of the superlattice reflections very difficult. Instead, fast Fourier transformations (FFTs) of different regions within the HAADF images were taken (ordered, high contrast; "disordered," low contrast). These yield similar results to diffraction patterns without the strong tilt dependence. In the FFTs, spatial frequencies consistent with $\{101\}$ superlattice reflections are visible in the high-contrast ordered regions of the HAADF images, as expected, while weak reflections are visible in the low-contrast regions, as seen in Figs. 1(c) and 1(d), respectively. This indicates that the regions exhibiting low contrast in the HAADF images were not regions of highly disordered Cr and Re sites but actually well-ordered regions separated by an antiphase boundary. This is an important distinction, because it helps to explain why the magnetic properties of the thin film SCRO were as notable as they were [21], in spite of seeing what appeared to be high degrees of B/B' disorder in HAADF images like Fig. 1(a). This shows that, through the direct interpretation of HAADF-STEM images of these films, information about the degree of B/B' ordering can be deduced at the extremes of ordering: fully ordered, completely disordered, and fully ordered domains separated by one or more antiphase boundaries.

To show how channeling allows one to distinguish between structures with different ordering and demonstrate what is possible, we have calculated the (integrated) HAADF signal on columns containing ten atoms in total (approximately 55 Å thick) for various compositions of Cr and Re atoms. Additionally, we have considered all the various possible orderings along the beam path, which is expected to further affect probe channeling. These results are shown in Fig. 3.

There is a clear and unambiguous distinction between the case where there is only a single Re or Cr atom in the specimen. Also, where that single atom is placed is in principle measurable, provided that an accurate measurement of the image contrast can be made (i.e., the bit depth of the image). Contrast this with the case where there are five Re atoms and five Cr atoms in the column: Now there are 252 possible permutations, and, although there is still a one-to-one relationship between a given arrangement of atoms and the measured signal, considerably more accuracy would be required to distinguish between the different configurations. It is also evident that as, say, the composition of the column changes and the number of Cr atoms increase there are ambiguities between the case of one and two atoms (10 and 20 at.% Cr, respectively) but not between one and three atoms. Nevertheless, by measuring the thickness of the specimen via position-averaged convergent beam electron diffraction [22] and the ratio of the two atomic species (using electron energy loss

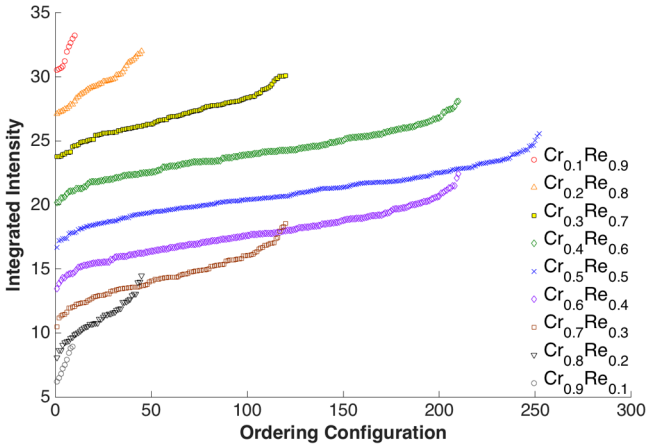

FIG. 3. Integrated HAADF intensity for different ratios (compositions) of Cr and Re atoms in a column of ten atoms taking into account the possible permutations of atoms in each case. Results have been ordered from the smallest to the largest cross section for each composition.

spectroscopy and/or energy dispersive x-ray spectroscopy) [27], it is clear that, as we have done in this Letter, useful information can be garnered by comparing the theory and experiment. The key point to realize is that the differences in Fig. 3 are due to differences in the channeling of the probe for different configurations, and it is this fact that provides useful information about the structure, in particular, between the different configurations for a given Cr to Re ratio. In a naïve model that ignores channeling, Fig. 3 would simply consist of a series of horizontal lines.

In Fig. 4, the calculated probe channeling profiles from the entrance surface (top) to the exit surface (bottom) for three different columns with identical compositions—50 Cr:50 Re—are displayed to show how atomic-scale ordering along the path of the beam affects probe channeling within the specimen and, thus, the observed HAADF-STEM intensities. Figure 4(a) shows that, for a column with all Cr near the entrance and Re near the exit surface, there is enhanced probe channeling. Figures 4(b) and 4(c) show the channeling for a column with alternating Cr and Re atoms and for one with all Re near the entrance surface and Cr near the exit surface, respectively. The column in Fig. 4(a) resulted in 15.9% and 21.7% higher HAADF intensity than that of Figs. 4(b) and 4(c), respectively. This can be attributed to a "prefocusing" effect that the lighter atoms near the entrance surface have on the probe. Because of this effect, the electron beam more strongly couples to the column, the second half of which has heavier Re atoms with larger scattering cross sections, resulting in higher HAADF intensity on such columns. The results in Figs. 4(a) and 4(c) are possible configurations that could be found in an antiphase domain such as that of Fig. 1, further demonstrating that quantitative STEM imaging is able resolve the difference between the two scenarios specifically due to the differences in probe channeling.

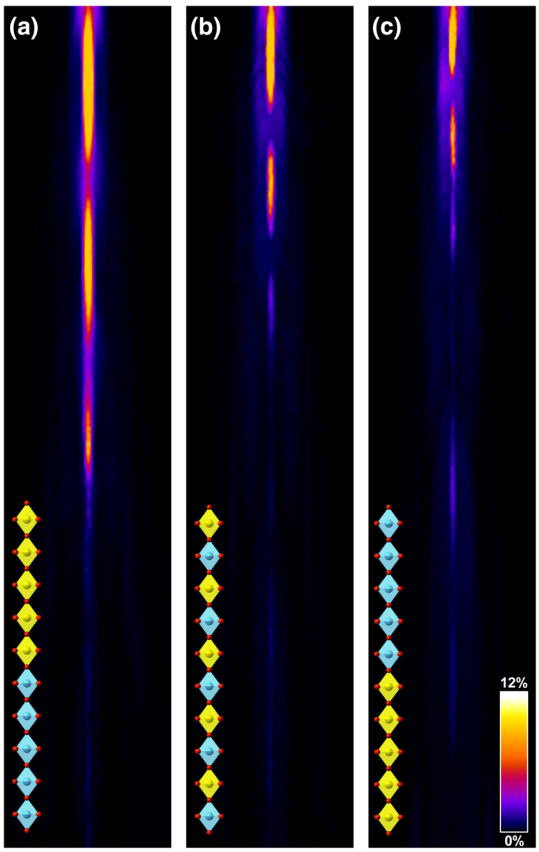

FIG. 4. Calculated scattering for a probe placed on three different 390 Å thick columns with identical compositions ($Cr_{0.5}Re_{0.5}$), where the top half of (a) is Cr with the bottom half Re atoms; (b) has Cr and Re atoms alternating; and the top half of (c) is Re with the bottom half Cr atoms. Oversized schematic structures are included in each panel to demonstrate the different types of ordering. Horizontal scale expanded 50× that of vertical scale for clarity. Color scale in percent probe current.

In order to fully quantify the experimental data, potential sources of error must be taken into account. One of the largest sources of error can be signal coming from neighboring columns due to thermally scattered electrons [28]. Thermal diffuse scattering can result in off-column contributions of signal that can affect not only HAADF-STEM images but also elemental maps. These effects can be accounted for by first quantifying experimental compositional maps in the manner of Chen *et al.* [27] together with simulations as described by Forbes *et al.* [28]. The resultant compositional maps can then be used to simulate HAADF-STEM intensities using larger cells with nearest and even next-nearest neighboring columns to include the contribution of thermally scattered electrons. Additionally, specimen preparation-induced amorphization or oxidation layers can increase the mean error in quantification by a few percent depending on the composition and thickness of the layer [29]. These effects can be minimized by mechanical wedge polishing and/or low-energy Ar ion milling to reduce or remove surface layers.

Fully quantitative HAADF-STEM imaging and spectroscopy has been demonstrated for sufficiently thin specimens, monatomic systems, and highly ordered compounds [14,15,27]. In particular, it has been successfully applied to locate impurity atoms in STO [15] for thin specimens of only a few layers thickness yet is a challenging proposition for thicker samples (greater than a few nanometers), especially if the material does not exhibit well-characterized ordering. Nevertheless, we have shown that using atomic resolution HAADF-STEM imaging, variations in column intensity can be used to distinguish the presence of random antisite disorder from that of antiphase boundaries in an otherwise highly ordered sample. Through the use of electron diffraction and image simulation, the low-contrast regions in Sr_2CrReO_6 thin films can clearly be shown to be antiphase domainlike in nature. The identification of antiphase domains within double perovskite thin films is pivotal in explaining differences in electronic and magnetic properties from their bulk values through the disruption of periodic superexchange couplings necessary for ferrimagnetism.

This work is supported by the Center for Emergent Materials at the Ohio State University, a National Science Foundation Materials Research Science and Engineering Center (Grant No. DMR-1420451). Partial support is provided by the Center for Electron Microscopy and Analysis and the NanoSystems Laboratory at the Ohio State University, as well as by an allocation of computing time from the Ohio Supercomputer Center. This research was supported under the Australian Research Councils Discovery Projects funding scheme (Project No. P110102228).

[1] H. Kato, T. Okuda, Y. Okimoto, Y. Tomioka, Y. Takenoya, A. Ohkubo, M. Kawasaki, and Y. Tokura, Appl. Phys. Lett. **81**, 328 (2002).
[2] D. Serrate, J. M. D. Teresa, and M. R. Ibarra, J. Phys. Condens. Matter **19**, 023201 (2007).
[3] M. G. Blamire, J. L. MacManus-Driscoll, N. D. Mathur, and Z. H. Barber, Adv. Mater. **21**, 3827 (2009).
[4] J. M. Lucy, M. R. Ball, O. D. Restrepo, A. J. Hauser, J. R. Soliz, J. W. Freeland, P. M. Woodward, W. Windl, and F. Y. Yang, Phys. Rev. B **90**, 180401 (2014).
[5] A. J. Hauser, R. E. A. Williams, R. A. Ricciardo, A. Genc, M. Dixit, J. M. Lucy, P. M. Woodward, H. L. Fraser, and F. Yang, Phys. Rev. B **83**, 014407 (2011).
[6] X. Yu, T. Asaka, Y. Tomioka, Y. Kaneko, M. Uchida, J. He, T. Nagai, K. Kimoto, Y. Matsui, and Y. Tokura, J. Magn. Magn. Mater. **310**, 1572 (2007).
[7] H. Asano, N. Kozuka, A. Tsuzuki, and M. Matsui, Appl. Phys. Lett. **85**, 263 (2004).
[8] S. Chakraverty, A. Ohtomo, and M. Kawasaki, Appl. Phys. Lett. **97**, 243107 (2010).
[9] S. Geprägs, F. Czeschka, M. Opel, S. Goennenwein, W. Yu, W. Mader, and R. Gross, J. Magn. Magn. Mater. **321**, 2001 (2009).
[10] J. Orna, L. Morellon, P. Algarabel, J. Pardo, C. Magen, M. Varela, S. Pennycook, J. D. Teresa, and M. Ibarra, J. Magn. Magn. Mater. **322**, 1217 (2010).
[11] M. Opel *et al.*, Phys. Status Solidi A **208**, 232 (2011).
[12] J. M. De Teresa, D. Serrate, C. Ritter, J. Blasco, M. R. Ibarra, L. Morellon, and W. Tokarz, Phys. Rev. B **71**, 092408 (2005).
[13] T. K. Mandal, C. Felser, M. Greenblatt, and J. Kübler, Phys. Rev. B **78**, 134431 (2008).
[14] J. M. LeBeau, S. D. Findlay, L. J. Allen, and S. Stemmer, Nano Lett. **10**, 4405 (2010).
[15] J. Hwang, J. Y. Zhang, A. J. D'Alfonso, L. J. Allen, and S. Stemmer, Phys. Rev. Lett. **111**, 266101 (2013).
[16] K. van Benthem, A. R. Lupini, M. P. Oxley, S. D. Findlay, L. J. Allen, and S. J. Pennycook, Ultramicroscopy **106**, 1062 (2006).
[17] C. Niu, A. J. Zaddach, A. A. Oni, X. Sang, J. W. Hurt, J. M. LeBeau, C. C. Koch, and D. L. Irving, Appl. Phys. Lett. **106**, 161906 (2015).
[18] H. Akamine, K. van den Bos, N. Gauquelin, S. Farjami, S. V. Aert, D. Schryvers, and M. Nishida, J. Alloys Compd. **644**, 570 (2015).
[19] T.-W. Lim, S.-D. Kim, K.-D. Sung, Y.-M. Rhyim, H. Jeen, J. Yun, K.-H. Kim, K.-M. Song, S. Lee, S.-Y. Chung, M. Choi, and S.-Y. Choi, Sci. Rep. **6**, 19746 (2016).
[20] K. Sato, J. G. Wen, and J. M. Zuo, J. Appl. Phys. **105**, 093509 (2009).
[21] A. J. Hauser, J. R. Soliz, M. Dixit, R. E. A. Williams, M. A. Susner, B. Peters, L. M. Mier, T. L. Gustafson, M. D. Sumption, H. L. Fraser, P. M. Woodward, and F. Y. Yang, Phys. Rev. B **85**, 161201 (2012).
[22] J. M. LeBeau, S. D. Findlay, L. J. Allen, and S. Stemmer, Ultramicroscopy **110**, 118 (2010).
[23] B. D. Forbes, A. V. Martin, S. D. Findlay, A. J. D'Alfonso, and L. J. Allen, Phys. Rev. B **82**, 104103 (2010).
[24] L. Allen, A. D'Alfonso, and S. Findlay, Ultramicroscopy **151**, 11 (2015).
[25] S. J. Pennycook and P. D. Nellist, *Scanning Transmission Electron Microscopy: Imaging and Analysis* (Springer, New York, 2011).
[26] J. M. LeBeau, S. D. Findlay, L. J. Allen, and S. Stemmer, Phys. Rev. Lett. **100**, 206101 (2008).
[27] Z. Chen, A. D'Alfonso, M. Weyland, D. Taplin, L. Allen, and S. Findlay, Ultramicroscopy **157**, 21 (2015).
[28] B. D. Forbes, A. J. D'Alfonso, R. E. A. Williams, R. Srinivasan, H. L. Fraser, D. W. McComb, B. Freitag, D. O. Klenov, and L. J. Allen, Phys. Rev. B **86**, 024108 (2012).
[29] K. Mkhoyan, S. Maccagnano-Zacher, E. Kirkland, and J. Silcox, Ultramicroscopy **108**, 791 (2008).